

1 **Reverse mutational scanning of spike BA.2.86 identifies the epitopes**
2 **contributing to immune escape from polyclonal sera**

3
4 Najat Bdeir¹, Tatjana Lüddecke¹, Henrike Maaß¹, Stefan Schmelz², Henning Jacobsen¹, Kristin
5 Metzdorf¹, Anne Cossmann³, Metodi V. Stankov³, Markus Hoffmann^{4,5}, Stefan Pöhlmann^{4,5},
6 Wulf Blankenfeldt^{2,6}, Alexandra Dopfner-Jablonka^{3,7}, Georg M.N. Behrens^{3,7,8,#}, Luka Čičin-
7 Šain*^{1,7,8,#}

8
9 ¹ Department of Viral Immunology, Helmholtz Centre for Infection Research Braunschweig,
10 Germany

11 ² Department Structure and Function of Proteins, Helmholtz Centre for Infection Research
12 Braunschweig, Germany

13 ³ Department of Rheumatology and Immunology, Hannover Medical School, Hannover,
14 Germany

15 ⁴ Infection Biology Unit, German Primate Center – Leibniz Institute for Primate Research,
16 Göttingen, Germany

17 ⁵ Faculty of Biology and Psychology, University Göttingen, Göttingen, Germany

18 ⁶ Institute for Biochemistry, Biotechnology and Bioinformatics, Technische Universität
19 Braunschweig, Braunschweig, Germany

20 ⁷ German Centre for Infection Research (DZIF), partner site Hannover-Braunschweig,
21 Hannover, Germany

22 ⁸ Centre for Individualized Infection Medicine, a joint venture of HZI and MHH, Hannover,
23 Germany

24 # shared senior authorship

25 *For correspondence: Luka Čičin-Šain: Luka.Cicin-Sain@helmholtz-hzi.de

NOTE: This preprint reports new research that has not been certified by peer review and should not be used to guide clinical practice.

26 **SUMMARY**

27 **The recently detected Omicron BA.2.86 lineage contains more than 30 amino acid**
28 **mutations relative to BA.2. Here, we identify the epitopes driving immune escape of**
29 **BA.2.86 and its derivative JN.1 (BA.2.86 + S455L) lineage. We investigated the cross-**
30 **reactive humoral immunity within a cohort of health care workers against Omicron**
31 **BA.2.86 and JN.1 by employing pseudo-viral mutants. We demonstrate that BA.2.86 and**
32 **especially JN.1 evaded neutralization by serum antibodies of fully vaccinated individuals.**
33 **To discern the contribution of individual epitope mutations to immune escape, we**
34 **constructed a library of 33 BA.2.86 mutants, each of which harbored a single revertant**
35 **mutation going back to BA.2. This library was used in a reverse mutational scanning**
36 **approach to define serum neutralization titers against each epitope separately. The**
37 **mutations within the receptor binding domain (RBD) at position K356T and to a lesser**
38 **extent the mutations N460K, V483Δ, A484K, and F486P enhanced the immune escape.**
39 **More surprisingly, the mutation 16insMPLF within the spike N-terminal domain (NTD)**
40 **and the mutation P621S in S1/S2 significantly contributed to antibody escape of BA.2.86.**
41 **Upon XBB.1.5 booster vaccination, neutralization titers against JN.1 and BA.2.86**
42 **improved relative to all ancestral strains, and the residual immune escape was driven by**
43 **mutations at positions 16insMPLF, Δ144Y, E544K, P621S, and A484K.**

44

45 INTRODUCTION

46 The emergence of new SARS-CoV-2 virus lineages continues to be a critical aspect of the
47 ongoing epidemic viral spread. Among these lineages, BA.2.86, also known as Pirola, has
48 garnered recent attention owing to its significant antigenic shift away from the prevailing XBB
49 sub-lineage (1, 2). The earliest detection of BA.2.86 was in late July 2023 in Denmark (3-5).
50 By mid-august, it had been detected within several countries and WHO had classified it as a
51 variant of interest (4-6). An outbreak of BA.2.86 recorded in the United Kingdom with a high
52 attack rate (86.6%) within an elderly care home demonstrated the transmissibility of this
53 lineage (7). At present, the extent of disease severity exerted by BA.2.86 is unclear, but its
54 derivative sub-variant JN.1 is on track to become the globally dominant SARS-CoV-2 lineage.
55 The viral spike (S) protein mediates SARS-CoV-2 host cell entry through a multistep process.
56 The initial step involves binding of the S protein to angiotensin converting enzyme-2 receptors
57 (ACE2). This engagement is followed by S protein cleavage by host cell proteases, enabling
58 the S protein to drive fusion of the viral envelope with cellular membranes (8). The S1 domain
59 of the S protein entails an N-terminal domain (NTD) with somewhat unclear functions, and the
60 receptor-binding domain (RBD), which directly binds to ACE2 and is the major target for
61 neutralizing antibodies (8-10). The transmembrane S2 domain drives viral fusion with the host
62 cell membrane, which facilitates the release of viral genetic material into the cytoplasm, and
63 therefore plays an important role in infection. BA.2.86 harbors more than 30 mutations relative
64 to BA.2, encompassing 13 mutations in NTD, 14 in the RBD, and 7 within the pre S1/S2 and
65 S2 domain (11). Furthermore, several BA.2.86 descendants have been identified, including
66 BA.2.86.1 (defining mutation ORF1a:K1973R), JN.1 (L455S), JN.2 (ORF1a:Y621C), JN.3
67 (ORF1a:T2087I), and BA.2.86.2 (ORF7a:E222D)(2).

68 The alarming number of BA.2.86 spike mutations has prompted several efforts to
69 characterize the antibody immune escape potential of this lineage. Recent studies demonstrate

70 reduced pseudo-virus neutralization of BA.2.86 and JN.1 in comparison to BA.2 and B.1
71 strains and that vaccination with the monovalent BNT162b2 XBB.1.5 adapted vaccine
72 significantly enhances neutralization of BA.2.86 pseudo virus by serum antibodies (12-14).
73 However, the contribution of single mutations to the immune escape of BA.2.86 remains
74 unclear. Mutational scanning approaches, where libraries of viruses with single amino acid
75 mutations in the spike protein are compared to the wild-type virus are powerful tools for the
76 identification of epitopes recognized by monoclonal antibodies (15-17), but polyclonal serum
77 antibodies recognize numerous epitopes simultaneously and redundantly. Therefore, mutating
78 one out of 33 epitopes on an ancestral background may only marginally decrease the serum
79 neutralizing activity if some among the remaining 32 epitopes are recognized by independent
80 antibody clones. To overcome this limitation, we cloned a library of 33 reversion mutants on
81 the BA.2.86 background, each harboring a single mutation reverting the position back to the
82 amino acid in BA.2. This approach allowed us to observe a robust increase in neutralizing
83 activity whenever an immunologically relevant epitope was reintroduced in the spike. We
84 tested this library of BA.2.86 mutants against serum samples collected from a cohort of 30
85 healthcare workers, before and after vaccination with the BNT162b2 XBB.1.5 adapted vaccine.
86 Our data showed that mutations ins16MPLF, K356T, N460K, V483Δ, A484K, F486P and
87 S621P distributed across NTD, RBD, and S1/S2 domains, contribute to the immune escape of
88 BA.2.86. Additionally, we show that vaccination with the BNT162b2 XBB.1.5 adapted
89 vaccine increases substantially the neutralization titers against both BA.2.86 and the more
90 recent BA.2.86.1.1 (JN.1) descendant, and that the immune escape of JN.1 is more pronounced
91 than that of BA.2.86 before, but not after XBB.21.5 booster vaccination. Moreover, we
92 demonstrate that the deletion of the MPLF insertion at position 16, the reinsertion of the
93 tyrosine residue at position 144, as well as the reversions K544E, S621P, and K484A improves
94 neutralization of BA.2.86 upon the XBB.1.5 booster shot.

95 RESULTS

96 BA.2.86 spike protein harbors a substantial amount of mutations within all domains

97 The analysis of the BA.2.86 spike sequence (specifically: hCoV-19/Denmark/DCGC-
98 647694/2023, EPI_ISL_18114953) revealed 33 mutations relative to BA.2 spike (Figure 1).
99 These include 13 mutations within the NTD, 14 mutations in the RBD, and 6 mutations within
100 the S2 and pre S1/S2 domain. Of these mutations, there are five deletions (H69 Δ , V70 Δ ,
101 Y144 Δ , N211 Δ , and V483 Δ) and one insertion after V16 (V16insMPLF). Among mutations
102 that have been previously identified in other variants of interest are R21T (B.1.617),
103 H69 Δ /V70 Δ (B.1.1.7/Alpha), Y144 Δ (XBB1.5; EG.5.1; BA.1), R158G (B.1.617.2/Delta),
104 E484K (B.1.351/Beta; P.1/Gamma) and P681R (B.1.617.2/Delta). Additionally, BA.2.86
105 harbors several mutations, which were rarely reported (V445H, N450D, N481K, V483 Δ ; and
106 E554K) (18-20). Among these mutations ins16MPLF, Δ Y144, F157S, R158G, H245N, A264D
107 are located within the NTD antigenic supersite and may contribute to immune escape (21).
108 Additionally, several mutations within the RBD of BA.2.86 have been associated with antibody
109 resistance including K356T, A484K, and N450D (9, 22, 23), while several other mutations
110 R493Q, F486P, N460K, and V483 Δ may alter ACE2 interactions (24, 25). Hence, BA.2.86
111 contains a plethora of mutations within the spike protein, which may alter key properties of
112 this virus in receptor binding and neutralizing antibody escape. To visualize the position of
113 mutations in the spike protein of BA.2.86 with respect to BA.2, we used
114 AlphaFold2/AlphaFold-Multimer (26, 27) to construct a structural model of the spike trimer of
115 BA.2.86. The model, which was obtained in a closed state with respect to the conformation of
116 the RBD, shows that mutations with respect to BA.2 are spread over the distal part of the
117 protein but otherwise do not cluster at specific positions (Fig. 1B-C).

118

119

120 **BA.2.86 and JN.1 efficiently escape antibody neutralization**

121 To assess the immune escape of the BA.2.86 and BA.2.86.1.1 (JN.1) lineages, we employed
122 pseudo-virus particles (pp) in neutralization assays. For comparison, we also included particles
123 harboring the spike protein of XBB.1.5 (XBB.1.5_{pp}), Wuhan-Hu-01 (WT_{pp}), BA.1 (BA.1_{pp}),
124 and BA.2 (BA.2_{pp}) (Figure 2A-B). We found that plasma obtained from a cohort of at least
125 double boosted individuals neutralized BA.1_{pp} and BA.2_{pp} with 2-fold and 3-fold reduced
126 efficiency as compared to the index WT_{pp}, respectively. However, the inhibition of BA.2.86_{pp}
127 and XBB.1.5_{pp} was 40- and 30-fold reduced, respectively (Figure 2A). Antibody escape of
128 JN.1_{pp} was even more pronounced, with an ~80-fold reduction relative to WT_{pp} (Figure 2A).
129 Plasma acquired post vaccination with the XBB.1.5-adapted mRNA vaccine neutralized
130 XBB.1.5_{pp}, BA.2.86_{pp}, and JN.1_{pp} with almost comparable efficiency, whereby the mean
131 neutralization titer was 6-fold, 11-fold, and 12-fold lower than WT_{pp}, respectively (Figure 2B).
132 Collectively, BA.2.86 and JN.1 escaped neutralization by antibodies induced upon primary
133 vaccination series and boosters with immunogens predating XBB lineages, whereby this escape
134 was more pronounced in JN.1. However, a vaccination with the XBB.1.5 adapted vaccine
135 boosted the neutralizing titers against both variants to similar extents, reduced the gap in
136 neutralization efficiency between them and Omicron BA.2, and eliminated it completely
137 between JN.1 and BA.2.86.

138 **Mutations ins16MPLF, K356T, N460K, V483Δ, A484K, F486P, and P621S contribute to** 139 **BA.2.86 neutralizing antibody escape.**

140 To investigate the effect of individual mutations within BA.2.86 on post-vaccination
141 neutralizing antibody escape, we cloned a comprehensive library of 33 individual BA.2.86
142 mutants. Each of them contains a single reversion relative to the amino acid sequence of BA.2,
143 while retaining the rest of the sequence as in BA.2.86. Geometric means of pseudo-virus

144 neutralization titers (PVNT50) against BA.2.86_{pp} were ~18-fold lower than against BA.2_{pp} prior
145 to vaccination with the XBB.1.5 vaccine (Figure 3A). Hence, we tested which mutations
146 decreased the gap between neutralization of BA.2_{pp} and BA.2.86_{pp}. Our data showed that
147 among the BA.2.86_{pp} mutants with single mutations within the NTD, only the insMPLF16 Δ _{pp}
148 reduced the gap to BA.2_{pp} to a mere 4-fold reduction (Figure 3A). The remaining NTD_{pp} single
149 mutants did not significantly contribute to neutralizing antibody escape, because their
150 neutralization titers were comparable to that of BA.2.86_{pp} (Figure 3B). While the N-terminus
151 of BA.2.86 spike protein is modelled with lesser confidence than the core of the structure
152 (Figure S1A-C), it is interesting that the N-terminal 16MPLF insertion is predicted to interact
153 with a crevice in the N-terminal domain (NTD; Figure S1B-C). This is reminiscent of SARS-
154 CoV spike protein (28), albeit here, the N-terminus is yet more extended and anchored via a
155 disulfide bridge to the core of the NTD (Figure S1D).

156 The neutralization capacity of serum samples against epitopes in the RBD of BA.2.86_{pp} was
157 significantly affected prior to the XBB.1.5 booster by the mutation K356T, which was ~3-fold
158 more efficiently neutralized than BA.2.86_{pp} (Figure 4A and 4B). Additionally, our results
159 showed that K460N_{pp}, Δ V483_{pp}, K484A_{pp}, and P486F_{pp} had a 7-, 8-, 8-, and 10-fold reduced
160 neutralization efficiency, respectively, relative to BA.2_{pp}, and thus much less than the 18-fold
161 reduction observed in BA.2.86_{pp}. While the latter results did not raise to statistical significance
162 over BA.2.86_{pp} (Fig. 4B), they indicated an improved neutralization in the presence of these
163 parental epitopes. In contrast, the remaining mutations within the RBD of BA.2.86 did not
164 enhance serum neutralization capacity.

165 In addition to the aforementioned RBD and NTD BA.2.86 mutants, we explored the
166 contribution of mutations within the S1/S2 and S2 regions to antibody evasion. We report a
167 significant increase in neutralization efficiency for BA.2.86 S621P_{pp}, whereby neutralization
168 efficiency of BA.2.86 S621P_{pp} was 3-fold lower than that of BA.2_{pp} and hence, significantly

169 higher than for BA.2.86_{pp} (Figure 5A and 5B) In contrast, BA.2.86 K554E_{pp}, V570A_{pp},
170 R681H_{pp}, F939S_{pp}, L1143P_{pp} all showed comparable neutralization sensitivity as compared to
171 BA.2.86_{pp} (Figure 5A, and 5B).

172 Interestingly, the impact of NTD mutations on neutralization escape following vaccination with
173 the adapted XBB.1.5 immunogen revealed that the mutants where the MPLF insertion at
174 position 16 was removed (insMPLF16 Δ _{pp}), or the reinsertion of the of the Y at position 144
175 (ins144Y_{pp}) recovered the neutralization efficiency of plasma samples to the level of BA.2
176 neutralization (Figure 6). A similar effect was observed for BA.2.86 mutants K554E_{pp} and
177 K484A_{pp}, which demonstrate neutralization efficiency comparable to BA.2_{pp} after XBB.1.5
178 booster vaccination. On the other hand, the neutralization of the BA.2.86 mutant S621P_{pp} was
179 not significantly increased after the XBB.1.5 booster vaccination (Figure 6). Since
180 neutralization efficiencies of BA.2.86_{pp} and JN.1_{pp} were comparable after the XBB.1.5 booster
181 vaccination, our data may argue that these positions are relevant for the residual immune escape
182 of JN.1 upon the XBB.1.5 booster as well.

183 Discussion

184 This work provides to our knowledge the first example of a reverse mutational scanning
185 strategy for the identification of epitopes that contribute to immune escape from vaccine-
186 induced immunity. Strategies based on mutational scanning of the SARS-CoV-2 spike are not
187 new. Others and us have shown that such approaches can be used to generate libraries
188 containing individual mutations present in the Omicron, but not in the ancestral variants, and
189 thus identify epitopes that escape recognition by monoclonal antibodies (16, 17) and polyclonal
190 sera (15, 16, 29). A very comprehensive mutational scanning based on the XBB.1.5 spike has
191 been recently performed by the Bloom lab to introduce 9000 theoretical mutations on the
192 XBB.1.5 background and thus predict future potential escape mutations (15). However,
193 forward mutational scanning cannot predict the emergence of lineages with big evolutionary

194 jumps, such as the Omicron BA.1 and BA.2.86 variants, where more than 30 mutations were
195 observed simultaneously, with no intermittent stages that are known. Moreover, such
196 approaches are not ideal for the analysis of neutralizing potential of polyclonal sera, where
197 redundant epitope recognition may result in virus neutralization even if immunologically
198 relevant epitopes are mutated. By reverse mutational scanning, we provide here a loss-of-
199 function genetic approach, allowing the identification of escape epitopes in polyclonal
200 responses to antigens with many simultaneous mutations. Thus, we identified a collection of
201 epitopes that contribute to immune escape from vaccine-induced immunity by BA.2.86 and its
202 derivative JN.1 lineage. This approach may also be rapidly deployed for subsequent lineages
203 with big evolutionary jumps that may emerge in the future.

204 The emergence of BA.2.86 harboring more than 30 mutations relative to BA.2 was reminiscent
205 of the Omicron appearance in 2021 and raised concerns regarding its antibody escape potential
206 (12, 13, 30). A number of these mutations (K356, V445, G446, N450, L452, and P621) were
207 also observed in omicron sub-lineages within immunocompromised patients. This may indicate
208 that reduced immune functions within some individuals may be a source of highly mutated
209 SARS-CoV2 lineages (31, 32). BA.2.86 has also evolved several descendants including JN.1
210 which harbors three mutations in non S-proteins and a hallmark S455L mutation in the spike
211 protein (2). In sera from a cohort that was at least double boosted, we observed that the S455L
212 mutation reduces the neutralization efficiency relative to BA.2.86 by a factor of ~ 2 , but that
213 the XBB.1.5 adapted vaccine booster increases neutralization efficiency against both lineages
214 to similar levels, which were merely 2-fold lower than the neutralization of Omicron XBB.1.5.
215 Nevertheless, their neutralization titers remain 5-6 fold lower than that of BA.2 following
216 vaccination, in line with data reported in Stankov et al. (33) and Wang et al. (13).

217 Several mutations within BA.2.86 significantly increased the neutralizing antibody escape
218 prior to vaccination with the adapted XBB.1.5 vaccine. We found that the NTD mutation

219 ins16MPLF significantly affected neutralization sensitivity, and its reversion resulted in a 4-
220 fold increase in neutralization titers relative to BA.2.86. While this region of the NTD is
221 disordered in published structures of the SARS-CoV-2 spike protein, indicating high intrinsic
222 flexibility, the MPLF insertion is somewhat reminiscent of the SARS-CoV spike protein, where
223 the N-terminus is yet more extended and anchored via a disulfide bridge to the core of the NTD
224 (Fig. S1D). It should be noted that several NTD-binding neutralizing antibodies have been
225 identified in the past (34, 35), indicating that mutations in this domain may indeed interfere
226 with the immune system's capacity to recognize the virus. Even more interestingly, we show
227 that the deletion of the MPLF insertion at position 16 or reinsertion of Y at position 144
228 increases neutralization efficiency after the adapted XBB.1.5 vaccination to BA.2 levels. Both
229 mutations are located within the NTD antigenic supersite, which is a key target for NTD
230 specific neutralizing antibodies (21). Moreover, in silico structural modeling of BA.2.86
231 performed by Colson et al. indicates that the MPLF insertion may mask a V-shaped
232 electronegative zone within the NTD, which is an unprecedented phenotype in SARS-CoV-2.
233 This zone may stabilize the virus onto target cells and may induce some long-range
234 conformational changes which affect the RBD with potential consequences on RBD-ACE2
235 interactions (36). However, our independent in silico analysis of this region of the NTD
236 structure argues that the changes at the N-terminal tip cannot be predicted with a high degree
237 of confidence. Therefore, the actual effects of this mutation on the NTD structure may only be
238 confirmed by empirical analysis in cryoelectron microscopy or similar approaches.

239 We also found that the mutation K356T within the RBD plays a contributing role to BA.2.86
240 escape of neutralization by polyclonal sera. This reduction in neutralization efficiency might
241 be attributed to the steric hindrance caused by the introduction of an additional glycosylation
242 site (37). Similarly, we demonstrate that mutations N460K, V483 Δ , A484K, and F486P within
243 the RBD enhance neutralizing antibody escape. This is in line with reports from Wang et al,

244 which show that mutation N460K and F486P shared in XBB.1.5 and EG.5.1 cause resistance
245 to class 1 and 2 monoclonal antibodies (mAb) (38). Structural modelling has shown that the
246 mutation N460K, which was first identified in BA.2.75, disrupts a hydrogen bond formed
247 between the RBD and a class 1 mAb (VH3-53) (39) and a study by Wang et al. demonstrated
248 that the mutation A484K within BA.2.86 reduced the neutralizing activity of a subset of class
249 3 mAbs (13). The mutation V483 Δ has seldom been reported in circulating strains. Full spike
250 mutational scanning of BA.2.86 postulated that V483 Δ may contribute to antibody escape but
251 experimental evidence for this has been lacking (15). Our data argue that such effects may be
252 present, albeit not very pronounced. We also show that the mutation P621S in the S1/S2 domain
253 of BA.2.86 contributed to significant neutralization escape and this phenotype, to our
254 knowledge has not been demonstrated previously. In sum, we have identified several mutations
255 that have significantly contributed to immune escape in our cohort. However, we cannot
256 exclude that additional mutations may result in immune escape in individuals whose repertoire
257 differs from our cohort of double boosted individuals. This requires additional studies in
258 cohorts of elderly people or those with immune deficiencies.

259 In sum, BA.2.86 and its JN.1 descendent efficiently escape neutralization by polyclonal
260 serum antibodies of double boosted individuals, and our data argue that this is due to
261 mutations at positions N460K, V483 Δ , A484K, F486P, K356T, P621S, and ins16MPLF. We
262 also observed that the S455N mutation provides a 2-fold increase in neutralization titres over
263 BA.2.86. However, neutralization titres of JN.1 and BA.2.86 were appreciably improved by
264 the XBB.1.5 vaccine booster to comparable levels. This may argue that the JN.1 lineage would
265 have no selective immunological advantage over BA.2.86 in an XBB.1.5-boosted population,
266 and that the residual immune escape of both lineages may rely on the shared epitopes at
267 positions ins16MPLF, Δ 144Y, E544K, P621S, and A484K.

268

269 **Limitations of the Study**

270 We have utilized the well-established pseudo-virus system to assess the contribution of single
271 mutations to the antibody escape potential of BA.2.86. While formal verification would require
272 the use of authentic SARS-CoV-2 with spike mutations introduced by reverse genetics,
273 neutralization titers in pseudo-viral and authentic virus setups have been shown to be
274 comparable due to the immunodominance of spike over other structural elements (40-42). An
275 additional limitation in our study is the lack of information regarding hybrid immunity within
276 our cohort, whereby some participants may have experienced a prior unrecorded infection with
277 XBB sublineages, which may have elicited a humoral immune response similar to vaccination.
278 However, only 4 individuals have a recorded infection in 2023, when the XBB.1.5 lineage was
279 present at high levels. Furthermore, the neutralization sensitivity of BA2.86 and BA.2.86
280 mutant viruses may vary due to the heterogeneity of immune background within our cohort
281 and maybe distinct to cohorts outside the scope of our present study, including elderly or
282 immunocompromised individuals. An additional limitation is that we have only analyzed a
283 library of single mutants and have not explored the impact of combinations of spike protein
284 mutations on serum neutralization.

285 **AUTHOR CONTRIBUTIONS**

286 Conceptualization: L.C-S.; Methodology: L.C-S; N.B; Investigation: N.B, T.L, H.M, K.M, H.J,
287 S.S; Formal analysis: N.B, S.S, W.B, L.C-S; Resources: S.P., M.H., A.D-J., and G.M.N.B;
288 Funding acquisition: L.C-S; Writing – original draft: N.B.; Writing – review & editing: all
289 authors.

290

291 **ACKNOWLEDGEMENTS:**

292 This research was funded by the Helmholtz Association through Helmholtz Campaign
293 COVIPA (KA1-Co-02) to L.C-S. and EU-Partnering grant MCMVaccine (PIE-008) to L.C-S.

294 and S.P. Funding to L.C-S and S.P. was also provided by the Ministry of Science and Culture
295 of Lower Saxony, through the COFONI Network, flex fund projects 6FF22 and 10FF22.

296 G.M.N.B. and A.D.-J. acknowledge funding from Ministry of Science and Culture of Lower
297 Saxony (14-76103-184, COFONI Network, project 4LZF23), G.M.N.B. acknowledges
298 funding by the European Regional Development Fund (ZW7-85151373), and A.D.-J.
299 acknowledge funding by European Social Fund (ZAM5-87006761).

300 We thank Ayse Barut, Yuliia Polianska, Inge Hollatz-Rangosch and Karina Watzke for expert
301 technical assistance, Natascha Gödecke for support with biosafety compliance and Gert
302 Zimmer (Institute of Virology and Immunology, Mittelhäusern, Switzerland) for providing the
303 VSV pseudo-virus system. We also thank the CoCo Study participants for their support and
304 the entire CoCo study team, especially Annika Heidemann and Luis Manthey, for technical
305 and logistical support.

306

307 **DECLARATION OF INTERESTS**

308 L.C-S. served as an advisor to Sanofi unrelated to this work. G.M.N.B. served as advisor for
309 Moderna unrelated to this work, A.D-J served as an advisor for Pfizer unrelated to this work,
310 S.P. and M.H. conducted contract research (testing of vaccinee sera for neutralizing activity
311 against SARS-CoV-2) for Valneva unrelated to this work. S.P. served as advisor for BioNTech,
312 unrelated to this work. H.J. served as advisor on COVID neutralization assays for WHO and
313 CEPI, unrelated to this work. The other authors declare no competing interests.

314

315

316 **Key Resources table**

317 **Table 1: Bacterial and virus strains**

| Bacteria or virus | Source | Catalogue number (N/A=not applicable) |
|--|---------------------------|--|
| VSV*ΔG-Fluc | Laboratory of Gert Zimmer | N/A |
| NEB [®] 10-beta Competent <i>E. coli</i> | New England BioLabs | C3019H |

318

319 **Table 2: Experimental Models- Cell lines**

| Cell line | Source | Catalogue number (N/A=not applicable) |
|-----------|--------|--|
| 293T | DSMZ | Cat# ACC-635; RRID: CVCL_0063 |
| Vero76 | ATCC | Cat# CRL-1586 |

320

321 **Table 3: Oligonucleotides**

| Oligos | Source | Catalogue number (N/A=not applicable) |
|---|---------------|--|
| SARS-2--S (D264A) F (gctTACTATGTGGGCTACCTGC) | Sigma-Aldrich | N/A |
| SARS-2--S (D264A) R (GGCGGCACCAGCTG) | Sigma-Aldrich | N/A |
| SARS-2-S (V570A) F (gccGATACCACAGACGCC) | Sigma-Aldrich | N/A |
| SARS-2-S (V570A) R (GATATCCCGGCCAAAC) | Sigma-Aldrich | N/A |
| SARS-2-S (K554E) F (gagAGCAACAAGAAGTTCCTGC) | Sigma-Aldrich | N/A |
| SARS-2-S (K554E) R (TGTCAGCACGCCGG) | Sigma-Aldrich | N/A |
| SARS-2-S (P486F) F (ttcAACTGCTACTTCCCAC) | Sigma-Aldrich | N/A |
| SARS-2-S (P486F) R (GCCCTTGCCCTTAC) | Sigma-Aldrich | N/A |
| SARS-2-S (H339G) F (ggcGAGGTGTTCAATGCC) | Sigma-Aldrich | N/A |
| SARS-2-S (H339G) R (GAAG | Sigma-Aldrich | N/A |
| SARS-2-S (S446G) F (ggcGGCAACTACGATTACTG) | Sigma-Aldrich | N/A |
| SARS-2-S (S446G) R (GTGTTTGGAGTCCAG) | Sigma-Aldrich | N/A |

| | | |
|--|---------------|-----|
| SARS-2-S (N245H) F (cacAGAAGCTACCTGACACC) | Sigma-Aldrich | N/A |
| SARS-2-S (N245H) R (CAGGGCCAGCAGTG) | Sigma-Aldrich | N/A |
| SARS-2-S (V332I) F (atcACCAATCTGTGCCC) | Sigma-Aldrich | N/A |
| SARS-2-S (V332I) R (ATTGGGGAACCGCAC) | Sigma-Aldrich | N/A |
| SARS-2-S (Δ insMPLF) F (ACCTGATCACAACAAC) | Sigma-Aldrich | N/A |
| SARS-2-S (Δ insMPLF) R (TCACACACTGGCTG) | Sigma-Aldrich | N/A |
| SARS-2-S (T356K) F (aagCGGATCAGCAATTGCG) | Sigma-Aldrich | N/A |
| SARS-2-S (T356K) R (CCGGTTCCAGGCGTAC) | Sigma-Aldrich | N/A |
| SARS-2-S (I212L) F (CACCCCTATCctgGGGCGGGATT) | Sigma-Aldrich | N/A |
| SARS-2-S (I212L) R (TGCTTGCTGTAGATCTTGAAG) | Sigma-Aldrich | N/A |
| SARS-2-S (F216L) F (ctgCCTCAGGGCTTCTCTG) | Sigma-Aldrich | N/A |
| SARS-2-S (F216L) R (ATCCCGCCCGATGATAG) | Sigma-Aldrich | N/A |
| SARS-2-S (W452L) F (ttgTACCGGCTGTTCCG) | Sigma-Aldrich | N/A |
| SARS-2-S (W452L) R (GTAATCGTAGTTGCCG) | Sigma-Aldrich | N/A |
| SARS-2-S (insN211) F (accTCGgGCGGGATtcc) | Sigma-Aldrich | N/A |
| SARS-2-S (insN211) R (tGATAGGGGTGTGCTTG) | Sigma-Aldrich | N/A |
| SARS-2-S (D450N) F (aatTACTGGTACCGGCTG) | Sigma-Aldrich | N/A |
| SARS-2-S (D450N) R (GTAGTTGCCGCTGTG) | Sigma-Aldrich | N/A |
| SARS-2-S (K460N) F (aacCTGAAGCCCTTCGAG) | Sigma-Aldrich | N/A |
| SARS-2-S (K460N) R (GGACTTCCGGAACAG) | Sigma-Aldrich | N/A |
| SARS-2-S (K481N) F (aacGGCAAGGGCCCAAC) | Sigma-Aldrich | N/A |
| SARS-2-S (K481N) R (ACAAGGCTTGTTGCCG) | Sigma-Aldrich | N/A |
| SARS-2-S (S621P) F (cccGTGGCCATTCACGC) | Sigma-Aldrich | N/A |
| SARS-2-S (S621P) R (CACTTCGGTACAGTTCAC) | Sigma-Aldrich | N/A |

| | | |
|--|---------------|-----|
| SARS-2-S (L1143P) F (cccGAGCTGGACAGCTTC) | Sigma-Aldrich | N/A |
| SARS-2-S (L1143P) R (CTGCAGAGGGTTCGTAC) | Sigma-Aldrich | N/A |
| SARS-2-S (Q493R) F (cggTCCTACGGCTTTCG) | Sigma-Aldrich | N/A |
| SARS-2-S (Q493R) R (CAGTGGGAAGTAGCAG) | Sigma-Aldrich | N/A |
| SARS-2-S (T21R) F (cgcACCCAGTCTACAC) | Sigma-Aldrich | N/A |
| SARS-2-S (T21R) R (TGTGATCAGGTTGAACAG) | Sigma-Aldrich | N/A |
| SARS-2-S (G158R) F (cggGTGTACAGCAGCGC) | Sigma-Aldrich | N/A |
| SARS-2-S (K158R) R (GGACTCGCTTCCATC) | Sigma-Aldrich | N/A |
| SARS-2-S (K403R) F (aggGGAATGAAGTGAGCC) | Sigma-Aldrich | N/A |
| SARS-2-S (K403R) R (GATCACGAAGCTGTC) | Sigma-Aldrich | N/A |
| SARS-2-S (L50S) F (agcACCCAGGACCTGTTC) | Sigma-Aldrich | N/A |
| SARS-2-S (L50S) R (GTGCAGCACGCTGG) | Sigma-Aldrich | N/A |
| SARS-2-S (F939S) F (ccAGCACAGCAAGCGC) | Sigma-Aldrich | N/A |
| SARS-2-S (F939S) F (CAGGCTGTCCTGGATC) | Sigma-Aldrich | N/A |
| SARS-2-S (L125V) F (gtCATCAAAGTGTGCGAGTTCC) | Sigma-Aldrich | N/A |
| SARS-2-S (L125V) F (CACGTTGGTGGCGTTG) | Sigma-Aldrich | N/A |
| SARS-2-S (H445V) F (gtcAGCGGCAACTACGATTAC) | Sigma-Aldrich | N/A |
| SARS-2-S (H445V) R (TTTGGAGTCCAGCTTG) | Sigma-Aldrich | N/A |
| SARS-2-S (S157F) F (ttcGGGGTGTACAGCAG) | Sigma-Aldrich | N/A |
| SARS-2-S (S157F) R (CTCGCTTCCATCC) | Sigma-Aldrich | N/A |
| SARS-2-S (insH69) F (cactCCGGCACCAATG) | Sigma-Aldrich | N/A |
| SARS-2-S (insH69) R (GATGGCGTGGAACCAg) | Sigma-Aldrich | N/A |
| SARS-2-S (insH70) F (gtctCCGGCACCAATG) | Sigma-Aldrich | N/A |
| SARS-2-S (insH70) R (GATGGCGTGGAACCAg) | Sigma-Aldrich | N/A |

| | | |
|---|---------------|-----|
| SARS-2-S JN.1 F (CTGGTACCGGagcTTCCGGAAGTC) | Sigma-Aldrich | N/A |
| SARS-2-S JN.1 R (TAATCGTAGTTGCCG) | Sigma-Aldrich | N/A |

322

323

Table 4: Recombinant DNA

| Recombinant DNA | Source | Catalogue number (N/A=not applicable) |
|--|-------------------------------|--|
| pCAGGS-DsRed | Laboratory of Stefan Pöhlmann | N/A |
| pCG1-SARS-2-SΔ18 BA.2.86 | Laboratory of Stefan Pöhlmann | N/A |
| pCG1-SARS-2-SΔ18 BA.2.86 S446G | Laboratory of Stefan Pöhlmann | N/A |
| pCG1-SARS-2-SΔ18 BA.2.86 F939S | Laboratory of Stefan Pöhlmann | N/A |
| pCG1-SARS-2-SΔ18 BA.2.86 Δ483Y | Laboratory of Stefan Pöhlmann | N/A |
| pCG1-SARS-2-SΔ18 BA.2.86 Δ144Y | Laboratory of Stefan Pöhlmann | N/A |
| pCG1-SARS-2-SΔ18 BA.2.86 K484A | Laboratory of Stefan Pöhlmann | N/A |
| pCG1-SARS-2-SΔ18 BA.2.86 R681H | Laboratory of Stefan Pöhlmann | N/A |
| Remaining pCG1-SARS-2-SΔ18 (BA2.86) single point mutants | Laboratory of Luka Cicin-Sain | N/A |

324

325

326

Table 5: Software and algorithms

| Software | Source | Version number |
|---------------------------|-----------------------|----------------|
| GraphPad Prism | GraphPad Software | 9.0 |
| Microsoft Office Standard | Microsoft Corporation | 2010 |

327

328 **Materials and Methods**

329 **Cell lines**

330 All cell lines were maintained at 37 °C and 5% CO₂ in a humidified environment. 293T (Human,
331 kidney) and VeroE6 (African green monkey, kidney) cells were cultured in Dulbecco's
332 Modified Eagle Medium (DMEM, ThermoFisher Scientific) supplemented with 5% fetal
333 bovine serum (FBS, ThermoFisher Scientific) and 100 U/ml penicillin and 0.1 mg/ml
334 Streptomycin (PAN-Biotec). Both cell lines were used to a maximum passage of 30. For
335 seeding and sub-cultivation, cells were washed with phosphate buffered saline (PBS, PAN-

336 Biotec) and then incubated with trypsin/EDTA (PAN-Biotec) until cell detachment. Cell lines
337 were routinely tested for mycoplasma. Transfection of 293T cells for the production of
338 pseudoviruses was carried out by calcium phosphate transfection.

339 **Plasmids**

340 The plasmid pCG1_SARS-2-Sdel18 (Codon-optimized) encoding the spike protein of the
341 Wuhan-Hu-1 SARS-CoV-2 has been previously reported (8). The pCG1_SARS-2-Sdel18
342 BA.1 and BA.2 expression plasmids are previously reported (29) and based on isolate hCoV-
343 19/Botswana/R40B58_BHP_3321001245/2021 (GISAID Accession ID: EPI_ISL_6640919)
344 and isolate hCoV-19/England/PHEC-4G0AFZF7/2021 (GISAID Accession ID:
345 EPI_ISL_8738174) respectively. The pCG1_SARS-2-Sdel18 XBB expression plasmid was
346 generated by Gibson assembly based on the expression vector for the spike of Omicron BA.2
347 and site directed mutagenesis was done to generate XBB.1.5. Expression plasmids pCAGGS-
348 DsRed and pCG1-SARS-2-SDel18 BA.2.86 (based on the isolate hCoV-19/Denmark/DCGC-
349 647694/2023, EPI_ISL_18114953) were kindly provided by the Laboratory of Stefan
350 Pöhlmann. Site directed mutagenesis (Q5® High-Fidelity 2X Master Mix, New England
351 BioLabs) was utilized for the generation of the SARS-CoV-2 spike BA.2.86 expression
352 plasmid library containing single point mutations back to BA.2 spike. Primers are listed in
353 **Table 3.**

354 **Production of Pseudo-viruses and titration**

355 Production of pseudo-viruses was performed according to published protocol (43). In brief,
356 293T cells were seeded in 6 well plates at a confluency of 70%. The next day, cells were
357 transfected with expression plasmids for pCG1-SARS-2-SΔ18 WT,
358 pCG1-SARS-2-SΔ18 BA2.86, pCG1-SARS-2-SΔ18 BA2, pCG1-SARS-2-SΔ18 BA2.86
359 XBB or pCG1-SARS-2-SΔ18 BA2.86 single point mutants. At 24 hours post transfection, cells
360 were incubated for 1 hour with a replication deficient VSV (VSV*ΔG) expressing enhanced

361 green fluorescent protein (eGFP) and firefly luciferase at an MOI of 3. Subsequently, cells were
362 washed with phosphate buffered saline (PBS) and incubated with anti-VSV-G antibody (mouse
363 hybridoma supernatant from CRL-2700; ATCC) in order to neutralize residual input virus. At
364 12 hours post infection, supernatants were harvested and cleared from cell debris by
365 centrifugation and stored at -80C for later use. All pseudo-viruses were titrated on VeroE6
366 confluent 96 well plates to ensure comparable infectivity according to a previously published
367 protocol (29).

368 **Neutralization assay**

369 Neutralization assays were based on a previously published protocol (29). All plasma samples
370 utilized in this study were heat inactivated at 56 °C for 30 minutes and stored at 4 °C for further
371 use. Pseudo-viral particles (600pfu/well± 30%) were incubated for one hour in a 96 well
372 microtiter plate with two-fold diluted serum samples in DMEM [1% Penicillin-Streptomycin,
373 1% L-Glu, 5% FBS] ranging from 1:10 to 1:5120. Pseudo-virus particles were incubated in the
374 absence of sera as controls indicating 0% inhibition. After incubation, the serum/virus samples
375 were transferred onto a confluent VeroE6 96 well plate. After a 24-hour incubation, plates were
376 fixed with 4% paraformaldehyde (PFA) and stored at 4 °C until readout. GFP+ infected cells
377 were counted using an IncuCyte S3 (Sartorius) performing whole-well scans (4x) in phase
378 contrast and green fluorescence settings (300ms exposure). Automated segmentation and
379 counting of fluorescent foci defined as green fluorescent protein GFP+-single cells was
380 performed using the IncuCyte GUI software (versions 2019B Rev1 and 2021B). Pseudo-virus
381 neutralization titer 50 (PVNT50) values were determined by a non-linear regression model.
382 The lower limit of confidence (LLOC) was set at a PVNT50 of 6.25 (dashed line). Non-
383 responders are defined as individuals below this threshold. All PVNT50 below 1 are set at 1
384 for visualization purposes. Due to technical limitations, sample numbers in our assays were
385 randomly distributed to have at least 20 individual sera within each group.

386 **Ethics committee Approval**

387 The collection of all plasma samples was approved by the research ethics committee of the
388 Institutional Review Board of Hannover Medical School (8973 BO K 2020). All donors
389 provided written consent for the blood donation and use for research purposes.

390 **Plasma Samples**

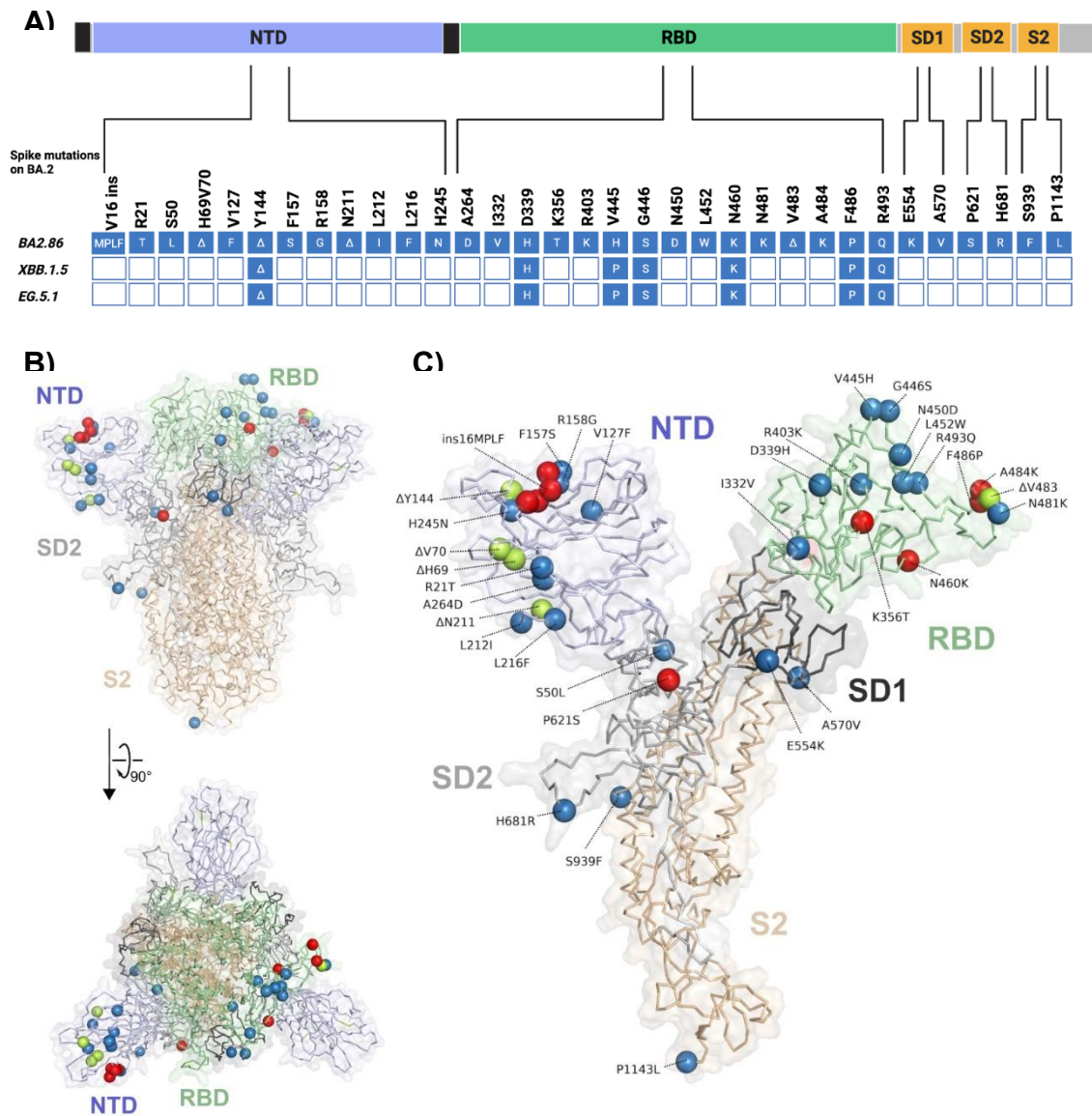
391 The number of participants within this analysis is n=30. Median age is 45 years (interquartile
392 range (IQR) 33 to 56.25) and mean age is 46 (SD=12.23). Male to female ratio is 1:3. Among
393 these participants, 30% were vaccinated with 3 vaccine doses, 63.3% were vaccinated with
394 four vaccine doses, and 6.6% were vaccinated with more than four doses. Ten participants
395 (33,3%) were vaccinated with the bivalent WT/BA.4/5 vaccine. The median time in months
396 since last recorded SARS-CoV-2 infection for the patients with known infection is 14.5 (IQR
397 10.75 to 18). The median number of months since the last known vaccination dates within our
398 cohort is 7 months (IQR 4 to 9). All participants are part of the COVID-19 contact study, to
399 monitor anti-SARS-CoV-2 immune responses in healthcare workers at the Hannover Medical
400 School (MHH). All participants donated blood directly prior to vaccination with 30µg of the
401 updated BNT162b2 Omicron XBB.1.5 vaccine (Raxtozinameran, BioNTech, Mainz,
402 Germany) in September 2023 and followed up for another blood collection two weeks post
403 vaccination (33). Plasma was separated from collected blood and stored at -80 °C for long term
404 storage and 4°C for immediate use. Detailed information is provided in **Supplementary table 1**.

405 **Statistical analysis**

406 Statistical analysis was performed using GraphPad Prism 9.0 (GraphPad software).
407 Neutralization titers were plotted as geometric mean titers. Data distribution was tested by
408 Shapiro-Wilks. A paired non-parametric Friedman test was performed for non-normally
409 distributed data. In normally distributed data, paired T-tests were performed. P values less than
410 0.05 were considered significant ns, $p > 0.05$; *, $p \leq 0.05$; **, $p \leq 0.01$; ***, $p \leq 0.001$).

411 FIGURES AND LEGENDS

Figure 1



412
413

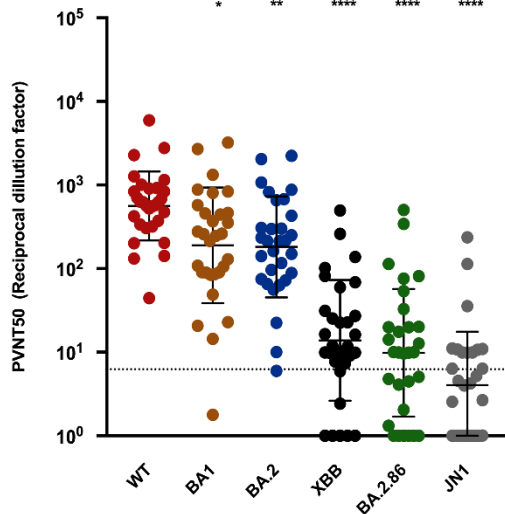
414 **Figure 1. Overview of BA.2.86 lineage specific spike protein mutations relative to BA.2**
 415 (A) Schematic representation of the SARS-CoV-2 spike domains and amino acid changes
 416 indicated for BA.2.86, and shared by XBB.1.5, and EG.5.1 compared to the spike of BA.2. N-
 417 terminal domain (NTD, blue), receptor binding domain (RBD, green), Subdomains 1 and 2
 418 (SD1 and SD2, orange), S2 subunit (orange). (B) Model of the trimeric spike protein of
 419 BA.2.86, calculated with AlphaFold2/AlphaFold-Multimer (27, 44). The N-terminal secretion

420 signal (15 residues) and the C-terminal membrane-anchoring sequence (112 residues) were
 421 omitted from calculations, leading to 3372 residues in the final model. Domains have been
 422 colored according to panel (A), and one of five independently calculated models is shown.
 423 Spheres represent the location of mutations with respect to the spike protein of BA.2. The
 424 positions of deletions are colored in green, red spheres indicate mutations that lead to enhanced
 425 immune escape of BA.2.86, other mutations are shown in blue. For clarity, mutations are only
 426 shown in one chain of the spike trimer. (C) Magnified view of one trimer extracted from the
 427 model shown in (B) and shown in the same orientation.
 428

Figure 2

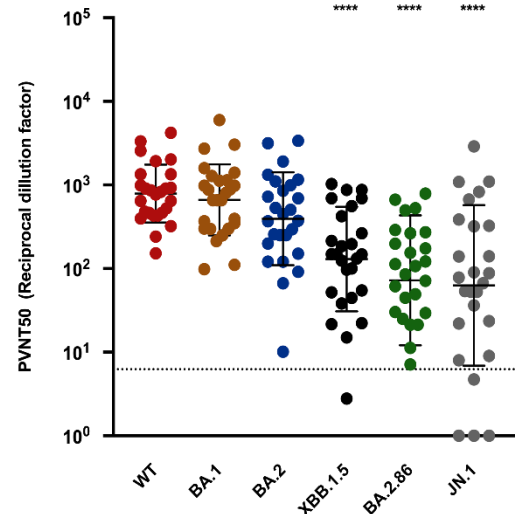
A) Before XBB.1.5 booster

| | | | | | | |
|-----------------------|--------|-------|-------|-------|-------|-------|
| Response rate: | 100% | 96.6% | 96.6% | 46.6% | 60% | 40% |
| Geometric mean titer: | 561.00 | 189.7 | 180 | 13.8 | 10.3 | 4.0 |
| Fold reduction (vs.): | — | 2.1x | 2.7x | 31.3x | 40.4x | 79.1x |
| | | * | ** | **** | **** | **** |



B) After XBB.1.5 booster

| | | | | | | |
|-----------------------|-------|-------|-------|-------|-------|-------|
| Response rate: | 100% | 100% | 100% | 96.6% | 96.6% | 85% |
| Geometric mean titer: | 787.6 | 663.8 | 394.3 | 130.0 | 72.31 | 62.93 |
| Fold change (vs.): | — | -x1.2 | -x2 | -x6 | -x11 | -x12 |
| | | | | **** | **** | **** |



429

430 **Figure 2. BA.2.86 and JN.1 efficiently evade neutralization in double boosted**
 431 **individuals, but the adapted XBB.1.5 vaccine booster enhances protection against both.**

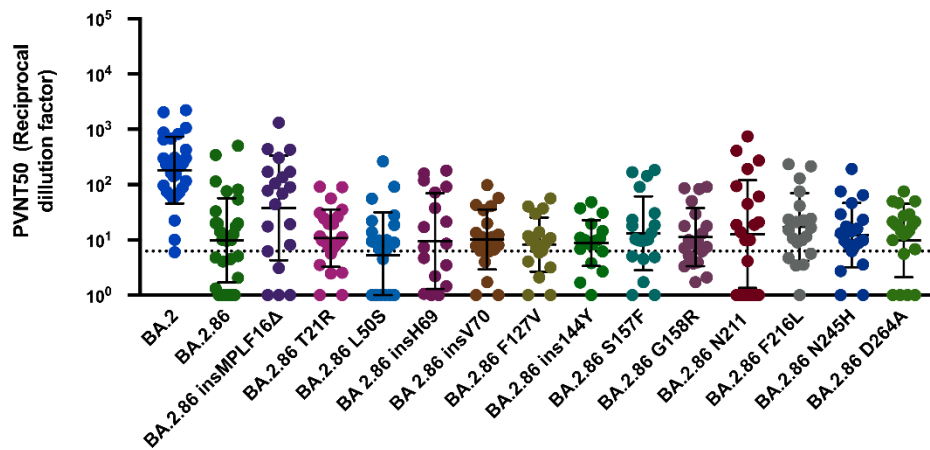
432 (A) Particles pseudo-typed with the indicated S proteins were pre-incubated for one hour at
 433 37 °C with sera dilutions from double boosted health care workers (n=30) (2A) or with
 434 plasma dilutions following vaccination with an adapted XBB.1.5 booster (n=26) (2B). Pseudo-

435 virus neutralization titer 50 (PVNT50) was calculated using the least squares fit using a variable
436 slope, using a four-parameter nonlinear regression model and values were plotted as geometric
437 mean. Geometric mean standard deviation bars are shown in black. The lower limit of
438 confidence (LLOC) was set at a PVNT50 of 6.25 (dashed line). Non responders are defined as
439 individuals below this threshold. All PVNT50 below 1 are set at 1 for visualization purposes.
440 The assay was performed in technical duplicates and with negative controls to assess the virus
441 input of each used pseudo-virus in the absence of plasma antibodies. Percentage of positive
442 responders, geometric means, and fold change neutralization over WT-Wuhan_{pp} are shown on
443 top. Friedman nonparametric paired test (ns, $p > 0.05$; *, $p \leq 0.05$; **, $p \leq 0.01$; ***, $p \leq 0.001$).
444 Percentage of positive responders, geometric means, and fold change neutralization over WT-
445 Wuhan_{pp} are shown on top.
446

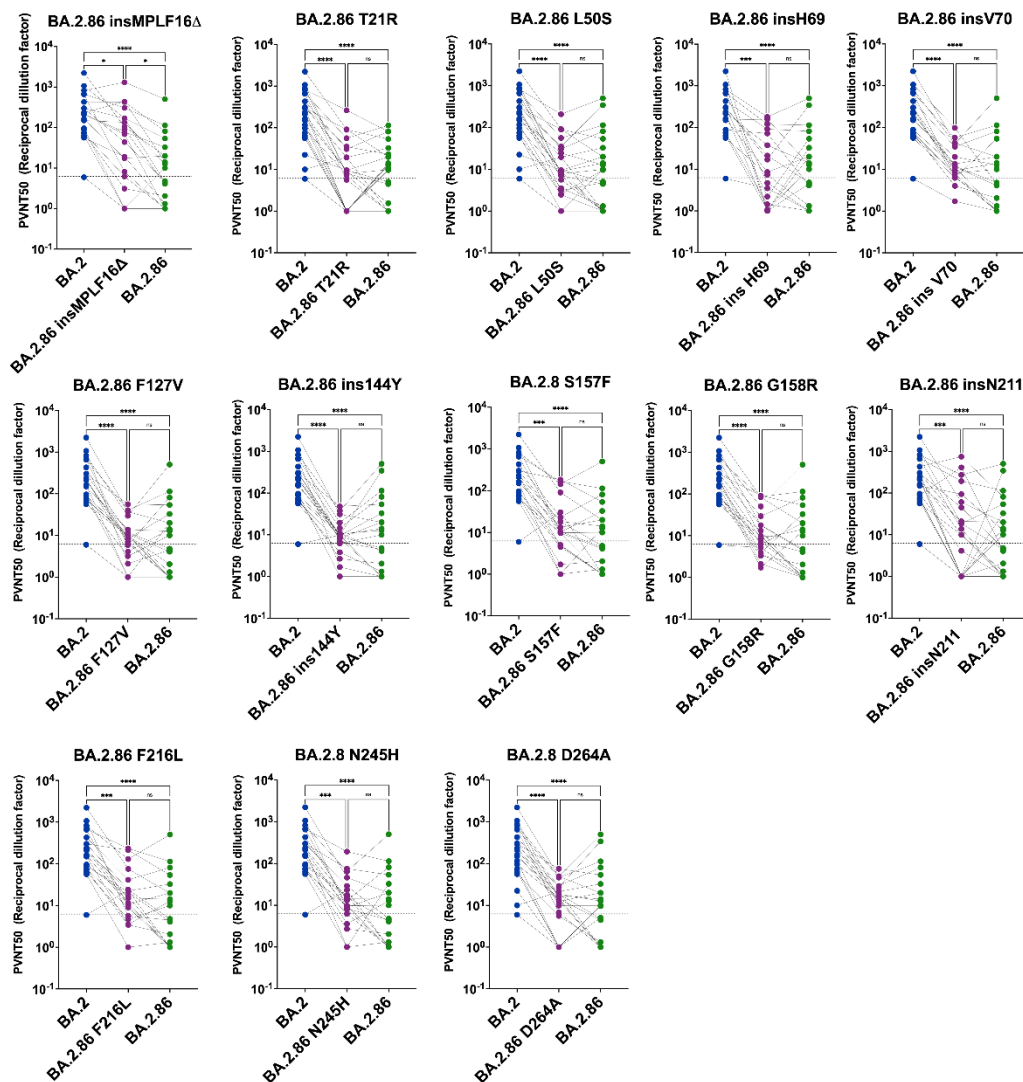
Figure 3

Neutralisation titers for NTD specific BA.2.86pp mutants pre XBB.1.5 adapted vaccine

A) Geometric mean titer: 180 10.3 44.9 10.72 5.3 9.5 10 8.2 8.7 13.2 11.2 12.7 17.4 12.2 9.97
 Fold change (vs.): — -18 -4.0 -17 -34 -19 -18 -22 -21 -14 -16 -14 -10 -15 -18
 Sample number: 30 30 20 25 25 18 21 19 20 20 20 21 20 20 23



B)



448 **Figure 3. Mapping mutations in the NTD for effects of neutralization efficiency of BA.2.86**
449 **in double boosted individuals**

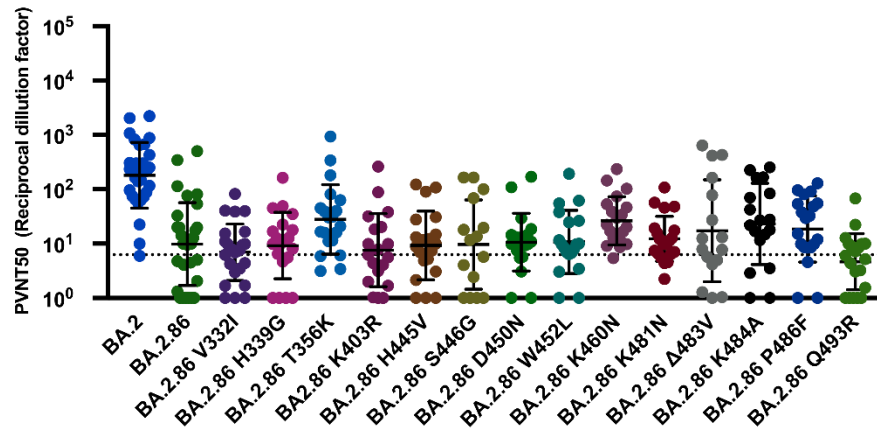
450 (A) Neutralization assessment for particles pseudo-typed with mutations within the NTD of
451 BA.2.86. Each mutant shown contains a single mutation reverting the amino acid mutation in
452 BA.2.86 to the corresponding amino acid within BA.2. Particles pseudo-typed with the
453 indicated S proteins were preincubated for one hour at 37 °C with sera dilutions from double
454 boosted health care workers with non-adapted immunogens. Pseudo-virus neutralization titer
455 50 (PVNT50) was calculated using the least squares fit using a variable slope, using a four-
456 parameter nonlinear regression model. The lower limit of confidence (LLOC) was set at a
457 PVNT50 of 6.25 (dashed line). Non responders are defined as individuals below this threshold.
458 All PVNT50 below 1 are set at 1 for visualization purposes. The assay was performed in
459 technical duplicates and with negative controls to assess the virus input of each used pseudo-
460 virus in the absence of plasma antibodies. Percentage of positive responders, geometric means,
461 and fold change neutralization over WT-Wuhan_{pp} are shown on top. Geometric mean standard
462 deviation bars are shown in black. (B) Individual neutralization data for particles pseudo-typed
463 with mutations within the NTD of BA.2.86. Statistical significance was assessed by Friedman
464 nonparametric paired test (ns, $p > 0.05$; *, $p \leq 0.05$; **, $p \leq 0.01$; ***, $p \leq 0.001$).

465

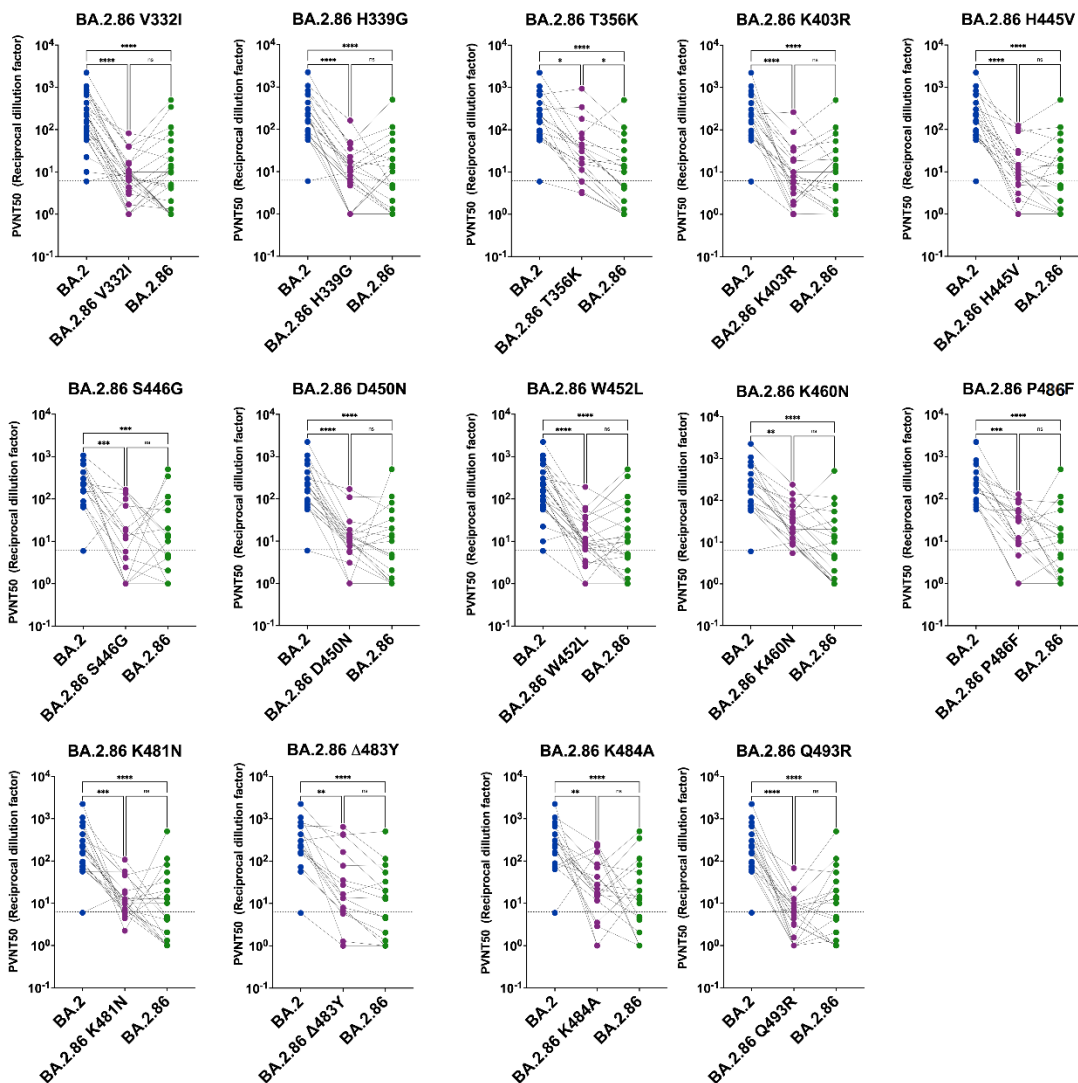
Figure 4

A) Neutralisation titers for RBD specific BA.2.86pp mutants pre XBB.1.5 adapted vaccine

| | | | | | | | | | | | | | | | | |
|-----------------------|-----|------|-----|-----|------|-----|-----|-----|------|------|------|------|------|------|------|-----|
| Geometric mean titer: | 180 | 10.3 | 6.7 | 9.2 | 28.0 | 7.6 | 9.2 | 9.6 | 10.6 | 10.7 | 26.3 | 12.3 | 22.8 | 23.0 | 18.6 | 4.6 |
| Fold reduction (vs.): | — | 18x | 27x | 20x | 6x | 24x | 20x | 19x | 17x | 17x | 7x | 15x | 8x | 8x | 10x | 39x |
| Sample number: | 30 | 30 | 25 | 20 | 20 | 19 | 20 | 15 | 20 | 19 | 20 | 21 | 17 | 18 | 20 | 20 |



B)



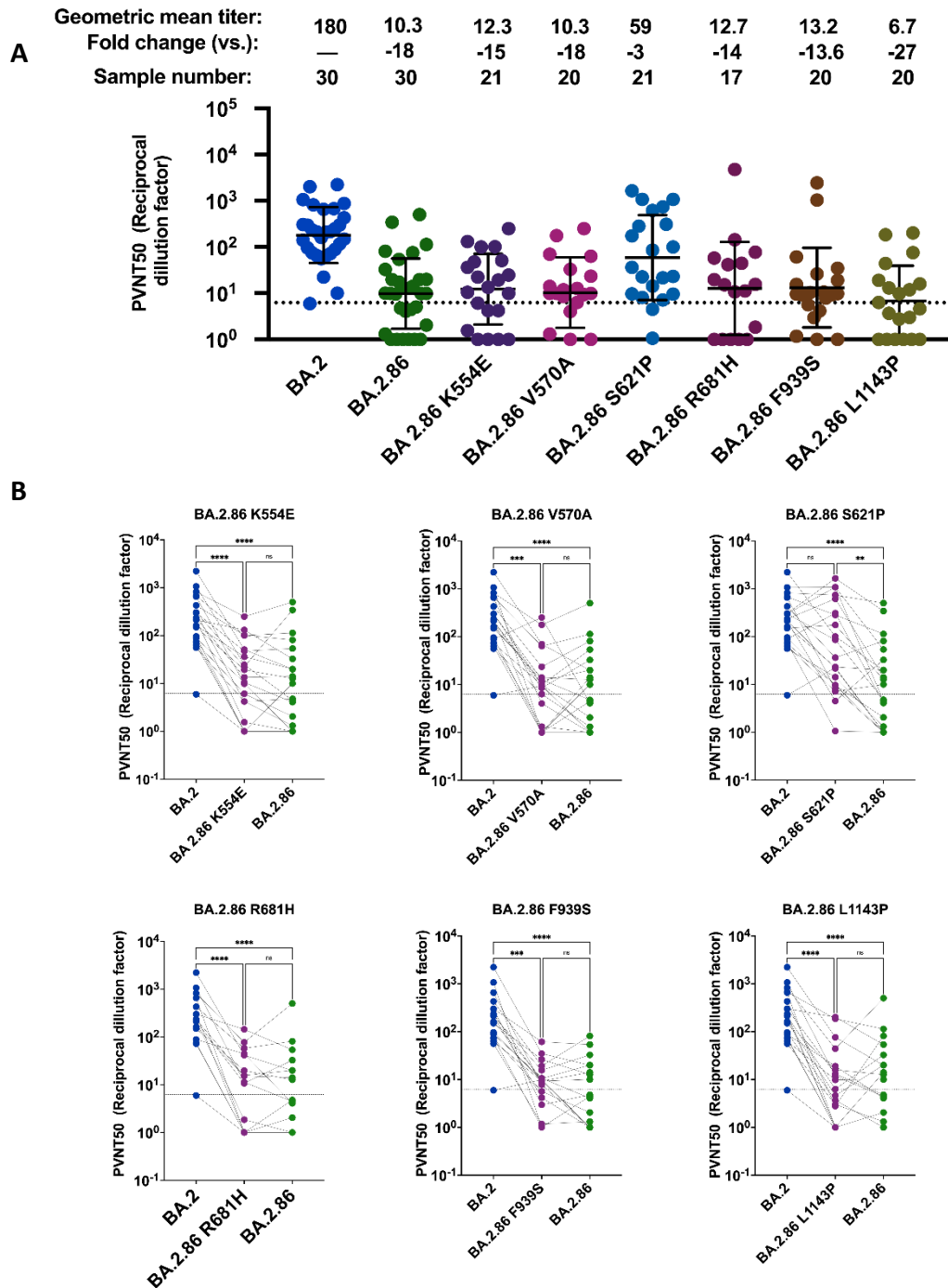
467 **Figure 4. Mutation K356T and to lesser extent K460N, ΔV483, K484A, and P486F within**
468 **the RBD enhance neutralization efficiency of BA.2.86 in double boosted individuals**

469 (A) Neutralization assessment for particles pseudo-typed with mutations within the RBD of
470 BA.2.86. Each mutant shown contains a single mutation reverting the amino acid mutation in
471 BA.2.86 to the corresponding amino acid within BA.2. Particles pseudo-typed with the
472 indicated S proteins were pre-incubated with serum dilutions from immunized health care
473 workers for one hour at 37 °C. Pseudo-virus neutralization titer 50 (PVNT50) was calculated
474 using the least squares fit using a variable slope, using a four-parameter nonlinear regression
475 model. The lower limit of confidence (LLOC) was set at a PVNT50 of 6.25 (dashed line). Non
476 responders are defined as individuals below this threshold. All PVNT50 below 1 are set at 1
477 for visualization purposes. The assay was performed in technical duplicates and with negative
478 controls to assess the virus input of each used pseudo-virus in the absence of plasma antibodies.
479 Percentage of positive responders, geometric means, and fold change neutralization over
480 BA.2_{pp} are shown on top. Geometric mean standard deviation bars are shown in black. (B)
481 Individual neutralization data for particles pseudo-typed with mutations within the RBD of
482 BA.2.86. Statistical significance was assessed by Friedman nonparametric paired test (ns, $p >$
483 0.05 ; *, $p \leq 0.05$; **, $p \leq 0.01$; ***, $p \leq 0.001$).

484

Figure 5

Neutralisation titers for S1/S2 and S2 specific BA.2.86pp mutants pre XBB.1.5



485

486 **Figure 5. Mutation S621P within the S1/S2 domain enhances neutralization efficiency of**
 487 **BA.2.86 in double boosted immunized individuals**

488 (A) Neutralization assessment for particles pseudo-typed with mutations within the S1/S2 and

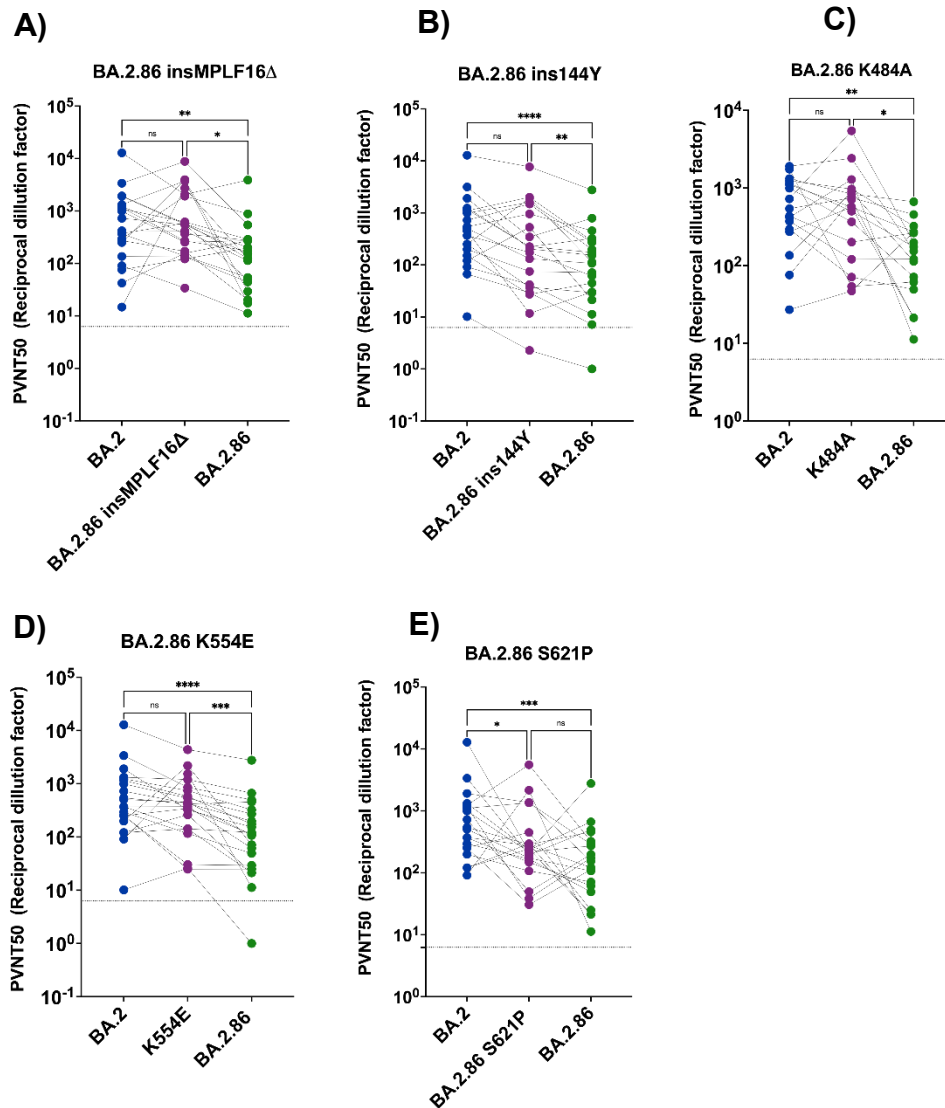
489 S2 domain of BA.2.86. Each mutant shown contains a single mutation reverting the amino acid

490 mutation in BA.2.86 to the corresponding amino acid within BA.2. Particles pseudo-typed with
491 the indicated S proteins were preincubated for one hour at 37 °C with sera dilutions from double
492 boosted health care workers with non-adapted immunogens. Pseudo-virus neutralization titer
493 50 (PVNT50) was calculated using the least squares fit using a variable slope, using a four-
494 parameter nonlinear regression model. The lower limit of confidence (LLOC) was set at a
495 PVNT50 of 6.25 (dashed line). Non responders are defined as individuals below this threshold.
496 All PVNT50 below 1 are set at 1 for visualization purposes. The assay was performed in
497 technical duplicates and with negative controls to assess the virus input of each used pseudo-
498 virus in the absence of plasma antibodies. Percentage of positive responders, geometric means,
499 and fold change neutralization over BA.2_{pp} are shown on top. Geometric mean standard
500 deviation bars are shown in black. (B) Individual neutralization data for particles pseudo-typed
501 with mutations within the S1/S2 and S2 domain of BA.2.86. Statistical significance was
502 assessed by Friedman nonparametric paired test (ns, $p > 0.05$; *, $p \leq 0.05$; **, $p \leq 0.01$; ***, p
503 ≤ 0.001).

504

Figure 6

Neutralisation titers for BA.2.86pp mutants post XBB.1.5 adapted vaccine



505

506 **Figure 6: Introduced mutations Δ insMPLF and Δ 144Y within BA.2.86 restores**
507 **neutralization capacity of sera post BNT162b2 XBB.1.5 vaccination to that of BA.2.**

508 (A-E) Neutralization assessment for pseudo-typed particles with sera post BNT162b2 XBB.1.5
509 vaccination. Each mutant shown contains a single mutation reverting the amino acid mutation
510 in BA.2.86 to the corresponding amino acid within BA.2. Particles pseudo-typed with the
511 indicated S proteins were pre-incubated for one hour at 37 °C with sera dilutions from double
512 boosted health care workers. Pseudo-virus neutralization titer 50 (PVNT50) was calculated

513 using the least squares fit using a variable slope, using a four-parameter nonlinear regression
514 model. The lower limit of confidence (LLOC) was set at a PVNT50 of 6.25 (dashed line). Non-
515 responders are defined as individuals below this threshold. All PVNT50 below 1 are set at 1
516 for visualization purposes. The assay was performed in technical duplicates and with negative
517 controls to assess the virus input of each used pseudo-virus in the absence of plasma antibodies.
518 Statistical significance was assessed by Friedman nonparametric paired test (ns, $p > 0.05$; *, p
519 ≤ 0.05 ; **, $p \leq 0.01$; ***, $p \leq 0.001$).
520

521 References

- 522 1. Callaway E. Why a highly mutated coronavirus variant has scientists on alert. *Nature*.
523 2023;620(7976):934.
- 524 2. Focosi D, Spezia PG, Maggi F. SARS-CoV-2 BA.2.86 ("Pirola"): Is it Pi or Just
525 Another Omicron Sublineage? *Vaccines (Basel)*. 2023;11(11).
- 526 3. Harris E. CDC Assesses Risk From BA.2.86, Highly Mutated COVID-19 Variant.
527 *Jama*. 2023;330(11):1029.
- 528 4. Rasmussen M, Møller FT, Gunalan V, Baig S, Bennedbæk M, Christiansen LE, et al.
529 First cases of SARS-CoV-2 BA.2.86 in Denmark, 2023. *Euro Surveill*. 2023;28(36).
- 530 5. Wannigama DL, Amarasiri M, Phattharapornjaroen P, Hurst C, Modchang C,
531 Chadsuthi S, et al. Tracing the new SARS-CoV-2 variant BA.2.86 in the community through
532 wastewater surveillance in Bangkok, Thailand. *Lancet Infect Dis*. 2023;23(11):e464-e6.
- 533 6. Lambrou AS, South E, Ballou ES, Paden CR, Fuller JA, Bart SM, et al. Early
534 Detection and Surveillance of the SARS-CoV-2 Variant BA.2.86 - Worldwide, July-October
535 2023. *MMWR Morb Mortal Wkly Rep*. 2023;72(43):1162-7.
- 536 7. Reeve L, Tessier E, Trindall A, Abdul Aziz NIB, Andrews N, Futschik M, et al. High
537 attack rate in a large care home outbreak of SARS-CoV-2 BA.2.86, East of England, August
538 2023. *Euro Surveill*. 2023;28(39).
- 539 8. Hoffmann M, Kleine-Weber H, Schroeder S, Krüger N, Herrler T, Erichsen S, et al.
540 SARS-CoV-2 Cell Entry Depends on ACE2 and TMPRSS2 and Is Blocked by a Clinically
541 Proven Protease Inhibitor. *Cell*. 2020;181(2):271-80.e8.
- 542 9. Lusvarghi S, Wang W, Herrup R, Neerukonda SN, Vassell R, Bentley L, et al. Key
543 Substitutions in the Spike Protein of SARS-CoV-2 Variants Can Predict Resistance to
544 Monoclonal Antibodies, but Other Substitutions Can Modify the Effects. *J Virol*.
545 2022;96(1):e0111021.
- 546 10. Zhou P, Yang XL, Wang XG, Hu B, Zhang L, Zhang W, et al. A pneumonia outbreak
547 associated with a new coronavirus of probable bat origin. *Nature*. 2020;579(7798):270-3.
- 548 11. Yang S, Yu Y, Jian F, Song W, Yisimayi A, Chen X, et al. Antigenicity and
549 infectivity characterisation of SARS-CoV-2 BA.2.86. *Lancet Infect Dis*. 2023;23(11):e457-
550 e9.
- 551 12. Uriu K, Ito J, Kosugi Y, Tanaka YL, Mugita Y, Guo Z, et al. Transmissibility,
552 infectivity, and immune evasion of the SARS-CoV-2 BA.2.86 variant. *Lancet Infect Dis*.
553 2023;23(11):e460-e1.
- 554 13. Wang Q, Guo Y, Liu L, Schwanz LT, Li Z, Nair MS, et al. Antigenicity and receptor
555 affinity of SARS-CoV-2 BA.2.86 spike. *Nature*. 2023.
- 556 14. Qian W, Yicheng G, Anthony B, Ian AM, Riccardo V, Carmen G, et al. XBB.1.5
557 monovalent mRNA vaccine booster elicits robust neutralizing antibodies against emerging
558 SARS-CoV-2 variants. *bioRxiv*. 2023:2023.11.26.568730.
- 559 15. Dadonaite B, Brown J, McMahon TE, Farrell AG, Asarnow D, Stewart C, et al. Full-
560 spike deep mutational scanning helps predict the evolutionary success of SARS-CoV-2
561 clades. *bioRxiv*. 2023.
- 562 16. Pastorio C, Zech F, Noettger S, Jung C, Jacob T, Sanderson T, et al. Determinants of
563 Spike infectivity, processing, and neutralization in SARS-CoV-2 Omicron subvariants BA.1
564 and BA.2. *Cell host & microbe*. 2022;30(9):1255-68.e5.
- 565 17. Abassi L, Bertoglio F, Mačak Šafranko Ž, Schirrmann T, Greweling-Pils M, Seifert
566 O, et al. Evaluation of the Neutralizing Antibody STE90-C11 against SARS-CoV-2 Delta
567 Infection and Its Recognition of Other Variants of Concerns. *Viruses*. 2023;15(11).

- 568 18. Miller J, Hachmann NP, Collier AY, Lasrado N, Mazurek CR, Patio RC, et al.
569 Substantial Neutralization Escape by SARS-CoV-2 Omicron Variants BQ.1.1 and XBB.1. N
570 Engl J Med. 2023;388(7):662-4.
- 571 19. Yue C, Song W, Wang L, Jian F, Chen X, Gao F, et al. ACE2 binding and antibody
572 evasion in enhanced transmissibility of XBB.1.5. Lancet Infect Dis. 2023;23(3):278-80.
- 573 20. Wang Q, Guo Y, Iketani S, Nair MS, Li Z, Mohri H, et al. Antibody evasion by
574 SARS-CoV-2 Omicron subvariants BA.2.12.1, BA.4 and BA.5. Nature. 2022;608(7923):603-
575 8.
- 576 21. McCallum M, De Marco A, Lempp FA, Tortorici MA, Pinto D, Walls AC, et al. N-
577 terminal domain antigenic mapping reveals a site of vulnerability for SARS-CoV-2. Cell.
578 2021;184(9):2332-47.e16.
- 579 22. Vellas C, Trémeaux P, Del Bello A, Latour J, Jeanne N, Ranger N, et al. Resistance
580 mutations in SARS-CoV-2 omicron variant in patients treated with sotrovimab. Clin
581 Microbiol Infect. 2022;28(9):1297-9.
- 582 23. Mykytyn AZ, Fouchier RA, Haagmans BL. Antigenic evolution of SARS coronavirus
583 2. Curr Opin Virol. 2023;62:101349.
- 584 24. Huo J, Dijokaite-Guraliuc A, Liu C, Zhou D, Ginn HM, Das R, et al. A delicate
585 balance between antibody evasion and ACE2 affinity for Omicron BA.2.75. Cell Rep.
586 2023;42(1):111903.
- 587 25. Qu P, Evans JP, Zheng YM, Carlin C, Saif LJ, Oltz EM, et al. Evasion of neutralizing
588 antibody responses by the SARS-CoV-2 BA.2.75 variant. Cell Host Microbe.
589 2022;30(11):1518-26.e4.
- 590 26. Tunyasuvunakool K, Adler J, Wu Z, Green T, Zielinski M, Židek A, et al. Highly
591 accurate protein structure prediction for the human proteome. Nature. 2021;596(7873):590-6.
- 592 27. Richard E, Michael ON, Alexander P, Natasha A, Andrew S, Tim G, et al. Protein
593 complex prediction with AlphaFold-Multimer. bioRxiv. 2022:2021.10.04.463034.
- 594 28. Yuan Y, Cao D, Zhang Y, Ma J, Qi J, Wang Q, et al. Cryo-EM structures of MERS-
595 CoV and SARS-CoV spike glycoproteins reveal the dynamic receptor binding domains.
596 Nature communications. 2017;8:15092.
- 597 29. Katzmarzyk M, Clesle DC, van den Heuvel J, Hoffmann M, Garritsen H, Pöhlmann
598 S, et al. Systematical assessment of the impact of single spike mutations of SARS-CoV-2
599 Omicron sub-variants on the neutralization capacity of post-vaccination sera. Front Immunol.
600 2023;14:1288794.
- 601 30. Sheward DJ, Yang Y, Westerberg M, Öling S, Muschiol S, Sato K, et al. Sensitivity
602 of the SARS-CoV-2 BA.2.86 variant to prevailing neutralising antibody responses. Lancet
603 Infect Dis. 2023;23(11):e462-e3.
- 604 31. Berkhout B, Herrera-Carrillo E. SARS-CoV-2 Evolution: On the Sudden Appearance
605 of the Omicron Variant. J Virol. 2022;96(7):e0009022.
- 606 32. Raglow Z, Surie D, Chappell JD, Zhu Y, Martin ET, Kwon JH, et al. SARS-CoV-2
607 shedding and evolution in immunocompromised hosts during the Omicron period: a
608 multicenter prospective analysis. medRxiv. 2023.
- 609 33. Stankov MV, Hoffmann M, Gutierrez Jauregui R, Cossmann A, Morillas Ramos G,
610 Graalman T, et al. Humoral and cellular immune responses following BNT162b2 XBB.1.5
611 vaccination. Lancet Infect Dis. 2023.
- 612 34. Chi X, Yan R, Zhang J, Zhang G, Zhang Y, Hao M, et al. A neutralizing human
613 antibody binds to the N-terminal domain of the Spike protein of SARS-CoV-2. Science (New
614 York, NY). 2020;369(6504):650-5.
- 615 35. Suryadevara N, Shiakolas AR, VanBlargan LA, Binshtein E, Chen RE, Case JB, et al.
616 An antibody targeting the N-terminal domain of SARS-CoV-2 disrupts the spike trimer. J
617 Clin Invest. 2022;132(11).

- 618 36. Colson P, La Scola B, Beye M, Delerce J, Raoult D, Fantini J. Emergence of a second
619 SARS-CoV-2 variant with a tremendous genetic leap from its ancestors. *J Med Virol.*
620 2023;95(10):e29124.
- 621 37. Wang Q, Li Z, Guo Y, Mellis IA, Iketani S, Liu M, et al. Evolving antibody evasion
622 and receptor affinity of the Omicron BA.2.75 sublineage of SARS-CoV-2. *iScience.*
623 2023;26(11):108254.
- 624 38. Wang Q, Iketani S, Li Z, Liu L, Guo Y, Huang Y, et al. Alarming antibody evasion
625 properties of rising SARS-CoV-2 BQ and XBB subvariants. *Cell.* 2023;186(2):279-86.e8.
- 626 39. Wang Q, Iketani S, Li Z, Guo Y, Yeh AY, Liu M, et al. Antigenic characterization of
627 the SARS-CoV-2 Omicron subvariant BA.2.75. *Cell Host Microbe.* 2022;30(11):1512-7.e4.
- 628 40. Lester S, Harcourt J, Whitt M, Al-Abdely HM, Midgley CM, Alkhamis AM, et al.
629 Middle East respiratory coronavirus (MERS-CoV) spike (S) protein vesicular stomatitis virus
630 pseudoparticle neutralization assays offer a reliable alternative to the conventional
631 neutralization assay in human seroepidemiological studies. *Access Microbiol.*
632 2019;1(9):e000057.
- 633 41. Tolah AMK, Sohrab SS, Tolah KMK, Hassan AM, El-Kafrawy SA, Azhar EI.
634 Evaluation of a Pseudovirus Neutralization Assay for SARS-CoV-2 and Correlation with
635 Live Virus-Based Micro Neutralization Assay. *Diagnostics (Basel).* 2021;11(6).
- 636 42. Quandt J, Muik A, Salisch N, Lui BG, Lutz S, Krüger K, et al. Omicron BA.1
637 breakthrough infection drives cross-variant neutralization and memory B cell formation
638 against conserved epitopes. *Sci Immunol.* 2022;7(75):eabq2427.
- 639 43. Berger Rentsch M, Zimmer G. A vesicular stomatitis virus replicon-based bioassay
640 for the rapid and sensitive determination of multi-species type I interferon. *PLoS One.*
641 2011;6(10):e25858.
- 642 44. Jumper J, Evans R, Pritzel A, Green T, Figurnov M, Ronneberger O, et al. Highly
643 accurate protein structure prediction with AlphaFold. *Nature.* 2021;596(7873):583-9.
- 644

645

646 **SUPPLEMENTARY INFORMATION**

647

648 **Table S1: Detailed information on the plasma samples.**

649

650 **Figure S1. Analysis of the structural model of the BA.2.86 spike protein**

651 (A) AlphaFold2/AlphaFold-Multimer model of the trimeric spike protein, colored by per-
652 residue model confidence score (pLDDT), with blue colors corresponding to high and red
653 colors corresponding to low confidence. The circle highlights the N-terminal domain NTD
654 further explored in the next panel. (B) The NTD of BA.2.86 spike protein colored by pLDDT
655 score. The circle highlights the N-terminal 16MPLF insertion of BA.2.86 and is further
656 explored in the next panel. (C) Predicted interactions of the 16MPLF insertion with a crevice
657 of the NTD. Colors correspond to the pLDDT score, N marks the position of the N-terminus
658 after cleavage of the signal peptide. (D) Comparison to the same region in the NTD of SARS-
659 CoV (PDB-ID 5X4S) (28). Note that this virus, with respect to SARS-CoV-2, carried an
660 extended N-terminus as well. Here, the N-terminus was anchored by a disulfide bridge (C19-
661 C133), which is not conserved in BA.2.86.

662